ARTICLE

Crystallization Behavior and Properties of B-Doped ZnO Thin Films Prepared by Sol-Gel Method with Different Pyrolysis Temperatures

Bin Wen[a], Chao-qian Liu[a*], Nan Wang[a], Hua-lin Wang[a], Shi-min Liu[a], Wei-wei Jiang[a], Wan-yu Ding[a], Wei-dong Fei[b,c*], Wei-ping Chai[a]

a. Engineering Research Center of Optoelectronic Materials & Devices, School of Materials Science and Engineering, Dalian Jiaotong University, Dalian 116028, China
b. School of Materials Science and Engineering, Harbin Institute of Technology, Harbin 150001, China
c. School of Mechanical Engineering, Qinghai University, Xining 810016, China

(Dated: Received on June 11, 2015; Accepted on August 14, 2015)

Boron-doped zinc oxide transparent (BZO) films were prepared by sol-gel method. The effect of pyrolysis temperature on the crystallization behavior and properties was systematically investigated. XRD patterns revealed that the BZO films had wurtzite structure with a preferential growth orientation along the *c*-axis. With the increase of pyrolysis temperature, the particle size and surface roughness of the BZO films increased, suggesting that pyrolysis temperature is the critical factor for determining the crystallization behavior of the BZO films. Moreover, the carrier concentration and the carrier mobility increased with increasing the pyrolysis temperature, and the mean transmittance for every film is over 90% in the visible range.

Key words: Transparent conduction oxide, Thin film, Boron-doped ZnO, Pyrolysis temperature, Sol-gel

I. INTRODUCTION

Zinc oxide (ZnO) is a direct wide band gap semiconductor with E_g=3.37 eV, and is naturally an n-type semiconductor due to oxygen vacancies and interstitial zinc atoms. In addition, ZnO is abundant, nontoxic, and stable in reducing atmosphere. It is considered as a promising candidate to replace indium tin oxide as transparent conducting electrodes in solar cell devices and flat panel display [1−3]. To enhance the electrical properties of ZnO, various atoms (*e.g.* Al, In, Ga, B, F) have been employed as donors [4−7]. Wherein, boron-doped ZnO has not only high transparency over the visible and near-infrared range, and low electrical resistivity, but also excellent light scattering property [8, 9]. Therefore, B-doped ZnO thin film has attracted some attention in recent years.

Generally, B-doped zinc oxide (BZO) thin films were primarily synthesized by chemical vapor deposition [10−15] and spray pyrolysis [16, 17]. Also, there are a few studies on the BZO thin films deposited by sol-gel method [18−23]. The sol-gel process has many advantages in preparing thin films, including low cost, excellent compositional control, easy handling and feasibility of deposition on large-area substrate [24]. In previous studies on the BZO films prepared by sol-gel process, the effects of annealing temperature [18], doping concentration of boron [19−23], and pH of precursor sol [1] on the crystallization, microstructure, electrical and optical properties of BZO films were reported systematically. To the best of our knowledge, the effect of pyrolysis temperature on the properties of BZO film has not been reported. In this work, BZO films were prepared by sol-gel spin coating and pyrolyzed at different temperatures, and the dependence of the properties of the BZO films on the pyrolysis temperatures was investigated.

II. EXPERIMENTS

Boron-doped ZnO precursor solution was prepared from zinc acetate di-hydrate ($Zn(Ac)_2{\cdot}2H_2O$, AR) and boric acid (H_3BO_3, GR) as sources for Zn and B, where the B/Zn atomic ratio was fixed at 0.5 at.%. The detailed solution preparation was described in our previous work [23]. The films were prepared by spin-coating the solution onto cleaned quartz glass substrates under 2000 r/min for 10 s at first. Then, each layer was directly put into a homemade tube furnace at 350−500 °C for 2 min to evaporate the solvent and pyrolyze organics, where the heating time from room temperature to pyrolysis temperature was 0.5 min. The details of the homemade tube furnace were also described in our previous work [25]. The spin-coating pyrolyzing procedure was repeated 5 times for each film. Finally, the deposited films were annealed at 500 °C for 5 min in Ar

*Authors to whom correspondence should be addressed. E-mail: cqliu@djtu.edu.cn, wdfei@hit.edu.cn

atmosphere. The thickness of all the films was about 160 nm measured by a step profiler (Veeco Dektak 6M).

The crystal structure of the films was analyzed by an X-ray diffractometer (PANalytical Empyrean) with Cu $K_{\alpha 1}$ radiation (λ=1.54056 Å) and a Göbel mirror at 40 kV and 40 mA, where the step size and the counting time were 0.05° and 0.5 s respectively. The surface morphologies of the thin films were characterized using an atomic force microscope (AFM, Bruker Multimode 8). A Hall effect measurement system (Swing HALL 8800) was employed to measure the electrical properties of the films. Optical transmittance measurements were performed by an ultraviolet-visible spectrophotometer (Hitachi U-3310) in the wavelength range from 300 nm to 900 nm.

III. RESULTS AND DISCUSSION

A. Structure

The XRD scan patterns of the BZO thin films pyrolyzed at different temperatures are shown in Fig.1(a). It is clear that the films exhibit a single-phase hexagonal structure (wurtzite ZnO JCPDS No.36-1451) and have the preferred orientation of (002) (*i.e.*, *c*-axis preferred orientation). Moreover, the intensity of (002) reflection was enhanced with increasing the pyrolysis temperature, suggesting that the pyrolysis temperature is the critical factor determining the crystallization behavior of the BZO films in the present work. To estimate the average grain size of the samples, the Scherers equation is employed:

$$D = \frac{0.89\lambda}{\beta \cos\theta} \tag{1}$$

where D is the grain size, λ is the X-ray wavelength of 1.54056 Å, θ is Bragg diffraction angle, and β is the full-width at half-maximum (FWHM) of the diffraction peak corresponding to 2θ. The FWHM values and calculated average grain sizes of the films pyrolyzed at different temperatures are shown in Fig.1(b). It is clear that the grain size increased with increasing the pyrolysis temperature.

B. Morphology

In order to understand deeply the influence of pyrolysis temperature on the crystallization behavior of the BZO films, the surface morphologies of the films were characterized by AFM in contact mode and are shown in Fig.2. From the two-dimensional AFM images, the combined tendency of the particles in the films can be clearly observed with increasing pyrolysis temperature. This result also suggests that the pyrolysis temperature is the critical factor for determining the crystallization behavior of the BZO films.

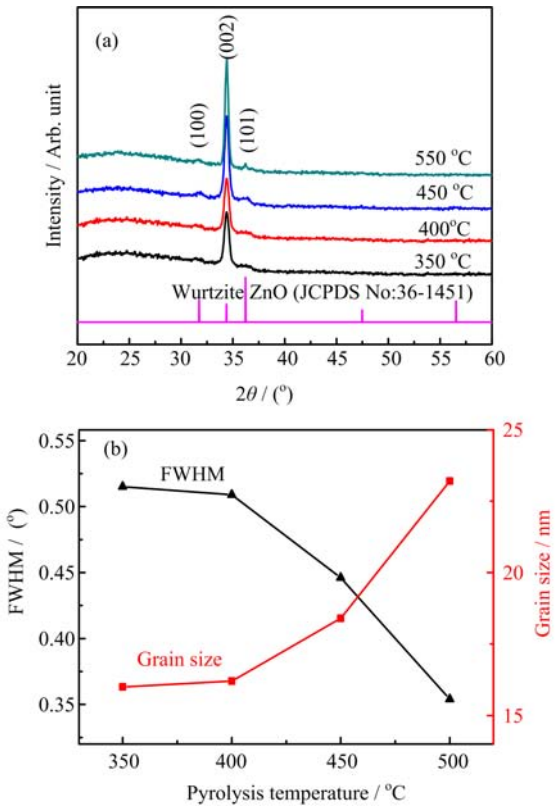

FIG. 1 (a) XRD 2θ scan patterns and (b) FWHM values and average crystallite sizes of the BZO films deposited at different pyrolysis temperatures.

The influence of the pyrolysis temperature on the growth behavior of the sol-gel derived BZO films can be understood on the basis of the understanding of the pyrolysis process. Primarily, the source material of $Zn(Ac)_2{\cdot}2H_2O$ involved in two chemical reaction processes in the precursor solution [26]. The first was a reversible hydrolysis reaction:

$$Zn(CH_3COO)_2 \cdot 2H_2O \leftrightarrow (ZnCH_3COO)^+ + CH_3COO^- + 2H^+ + 2OH^- \tag{2}$$

Then hydrolysis products reacted with monoethanolamine in the solvent of 2-methoxyethanol through the following chemical reaction:

$$CH_3COOZn^+ + CH_3COO^- + 2H^+ + 2OH^- + NH_2CH_2CH_2OH \rightarrow Zn(OH)_2 + CH_3COONH_2 + CH_3COOCH_2CH_3 + H_2O \tag{3}$$

Evidently, the reaction resultant of $Zn(OH)_2$ in the precursor solution is the source of the primary sol particles, and then can form the gel network in the spin-coating processes and can be adsorbed onto the substrate to form precursor film. According to the previous studies [27, 28], it can be known that the organic solvents and reaction resultants in the precursor film

DOI:10.1063/1674-0068/29/cjcp1506116

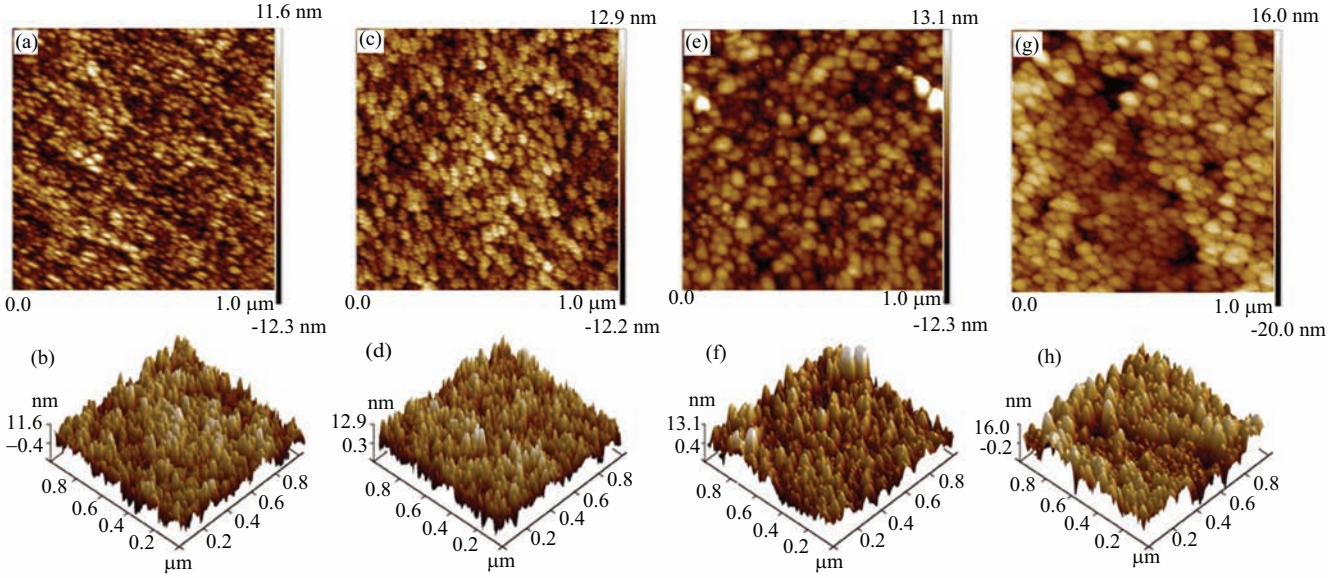

FIG. 2 Two- and three-dimensional AFM images of the BZO films deposited at (a, b) 350 °C, (c, d) 400 °C, (e, f) 450 °C, (g, h) 500 °C

can be entirely evaporated or pyrolyzed at the pyrolysis temperature below 350 °C. Moreover, the decomposition temperatures of $Zn(OH)_2$ and H_3BO_3 are about 125 and 185 °C, respectively. The above discussion indicates that there should not be any residual organic component or other volatile matter in the as-pyrolyzed films. Kang *et al.* [29] considered that the residual organic components in the as-pyrolyzed films would suppress the crystal growth of the films. Therefore, in our present work, the effect on the particle size in the annealed films should be controlled mainly by the pyrolysis temperature.

As for the further understanding about the effect of the pyrolysis temperature on the growth behavior of the sol-gel derived BZO films, it is described as the following. It is clear that the particle size is very small and less than 20 nm in diameter in the film pyrolyzed at 350 °C shown in Fig.2(a). Thus it can be reasonably deduced that the sol particle size in the precursor solution should be smaller than 20 nm. As is well known, generally, the smaller the nanoparticle size is, the higher the specific surface energy of the nanoparticle is. Therefore, in the pyrolysis process for preparing the BZO films, the sol particles in the precursor films were easy to merge, and the merging process was susceptible to the pyrolysis temperature. However, the grain growth in the as-pyrolyzed films was difficult in the post annealing process at 500 °C for 5 min. Generally, the grain growth due to post annealing corresponds to a recrystallization process. When the annealing temperature and time is not high or long enough, the grain growth is difficult. Therefore, although the as-pyrolyzed BZO films were annealed at 500 °C for 5 min, the particle size in the films was still mainly controlled by the pyrolysis

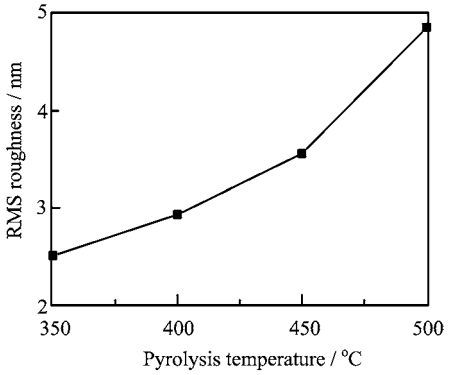

FIG. 3 RMS roughness of the BZO films deposited at different pyrolysis temperatures.

temperature. From that discussed above, we think the pyrolysis temperature is the critical factor affecting the crystallization behavior of the BZO films.

The root-mean-square (RMS) roughness of the BZO thin films is shown in Fig.3. It can be seen that the RMS roughness of the thin films increased with increasing pyrolysis temperature. Namely, the RMS roughness value of the BZO film pyrolyzed at 350 °C was about 2.5 nm, and then that of the BZO film pyrolyzed at 500 °C increased to about 4.9 nm. Evidently, the increase of the RMS roughness originated from the grain growth with increasing pyrolysis temperature.

C. Electrical properties

Hall measurements were carried out at room temperature to investigate the electrical properties of BZO

DOI:10.1063/1674-0068/29/cjcp1506116

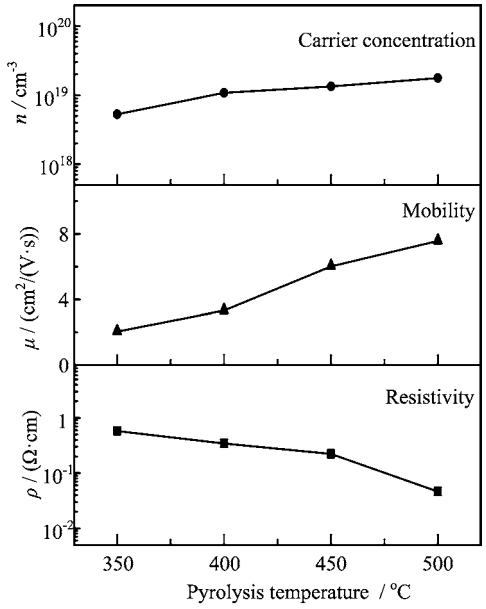

FIG. 4 Electrical properties of the BZO films as a function of the pyrolysis temperature.

films. The resistivity, Hall carrier concentration, and mobility of the films as a function of the pyrolysis temperatures are presented in Fig.4. When the pyrolysis temperature was raised from 350 °C to 500 °C, the carrier concentration of the BZO films increased from 5.27×10^{18} cm^{-3} to 1.77×10^{19} cm^{-3}, and the carrier mobility increased from 2.04 cm^2/(V·s) to 7.58 cm^2/(V·s). The increases in the carrier concentration and mobility should be attributed to the crystallization enhancement with increasing pyrolysis temperature. Logically, when the crystalline state of the sample of B-doped ZnO is poor, there will be a large amount of amorphous ZnO and boron oxide in the sample. The crystallization enhancement means more B atoms were doped into the crystal lattice of ZnO to replace the Zn^{2+}, and then more free charge carrier was released. As a result, the carrier concentration increased with increasing pyrolysis temperature. Moreover, the crystallization enhancement also means the defect concentration in the films decreased with increasing pyrolysis temperature. Correspondingly, the carrier mobility of the BZO films increased with increasing pyrolysis temperature. At the pyrolysis temperature of 500 °C, the BZO film has the lowest resistivity (4.64×10^{-2} Ω·cm) in the present work.

D. Optical properties

The transmittance spectra (T) of the BZO films were measured at room temperature by an ultraviolet-visible spectrophotometer, and are shown in Fig.5(a). All the transmittance spectra show mean values higher than 90% in the visible range. Moreover, it can be observed that the mean transmittances of the films in the visible range are fluctuant with pyrolysis temperature. The mean transmittance of the film pyrolyzed at 350 °C was lower than that of the film pyrolyzed at 400 °C in the visible range, which may be attributed to the difference in the crystalline states of the two films. According to the calculated grain size shown in Fig.1(b) and the two-dimensional AFM images shown in Fig.2, the crystalline state of the film pyrolyzed at 350 °C was slightly weaker than that of the film pyrolyzed at 400 °C. Therefore, the defect concentration in the former was higher than that in the latter, and then the mean transmittance of the former was lower than that of the latter in the visible range. When the the pyrolysis temperature exceeded 400 °C, the mean transmittance decreased with increasing pyrolysis temperature, which should be due to the increase of carrier concentration with increasing pyrolysis temperature. Generally, the higher the free carrier concentration is, the more serious the free carrier absorption and reflection in the visible range are. Therefore, according to the Hall measurement results, the mean transmittance of transmittance of the films pyrolyzed at higher temperature is lower in the visible range.

Generally, boron-doped ZnO is considered as a direct energy gap semiconductor, thus the relationship among absorption coefficient, photon energy, and optical band gap is

$$(\alpha h\nu)^2 = A\,(h\nu - E_{\rm g}) \tag{4}$$

where A is a constant for a direct transition, $h\nu$ is photon energy, α is the optical absorption coefficient, and $E_{\rm g}$ is the optical energy gap. To identify α for the BZO films, Lambert's law is used:

$$\alpha = \frac{1}{d}\ln\frac{1}{T} \tag{5}$$

where d is the film thickness and T is the transmittance spectra. The $E_{\rm g}$ was obtained by extrapolating downwards the corresponding straight lines till the intersection with energy axis, as shown in Fig.5(b). The determined optical band gaps are shown in the inset of Fig.5(b). The slight blue-shift in optical energy gap is clear with increasing the pyrolysis temperature. The increase in optical band gap of the BZO thin films should be attributed to Burstein-Moss effect.

IV. CONCLUSION

We have investigated the effect of pyrolysis temperature on the crystallization behavior, electrical and optical properties of sol-gel-derived boron-doped ZnO (BZO) films, and found that pyrolysis temperature was a critical factor affecting the crystallization behavior of the sol-gel-derived BZO films. XRD patterns revealed that all the BZO films had wurtzite structure with a preferential growth orientation along the c-axis. With increasing the pyrolysis temperature, the grain size of

DOI:10.1063/1674-0068/29/cjcp1506116

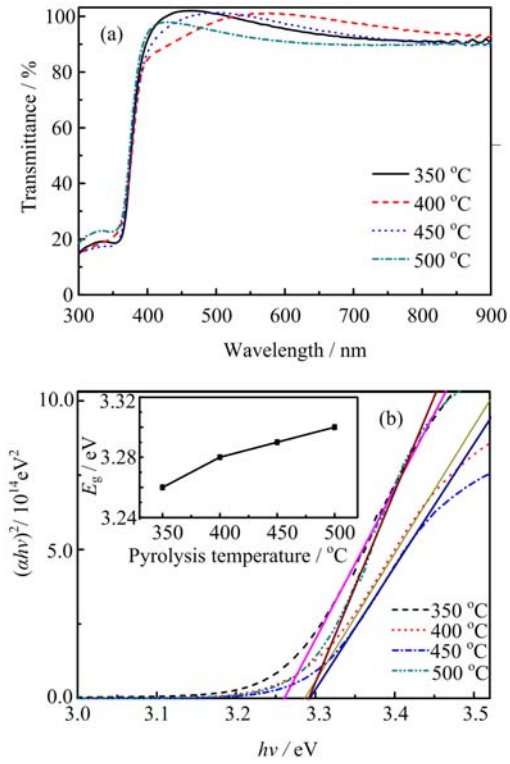

FIG. 5 (a) Transmittance spectra and (b) $(\alpha h\nu)^2$ versus $h\nu$ plot of the BZO films deposited at different pyrolysis temperatures. Inset: the optical band gap of the films.

the BZO films increased, and the RMS roughness of the films also increased. The mean transmittance for every film was over 90% in the visible range, and the optical band edge of the BZO films exhibited blue shift with increasing pyrolysis temperature. Moreover, with increasing pyrolysis temperature, the carrier concentration and the carrier mobility increased.

V. ACKNOWLEDGMENTS

This work was supported by the National Natural Science Foundation of China (No.51302024, No.51002018 and No.51472039), the Program for Liaoning Excellent Talents in University (No.LJQ2012038), the Higher Specialized Research Fund for the Doctoral Program (No.20122124110004), the Project of Education Department of Liaoning Province (No.L2013179), the Project of Open Research Foundation of State Key Laboratory of Advanced Technology for Float Glass (No.KF1301-01), the Dalian Science and Technology Plan Project (No.2011A15GX025), the Dalian Science and Technology Plan Project (No.2010J21DW008), and the Qinghai Province Science and Technology Project (No.2012-Z-701).

[1] B. Houng, C. L. Huang, and S. Y. Tsai, J. Cryst. Growth **307**, 328 (2007).
[2] A. Banejee and G. Guha, J. Appl. Phys. **69**, 1030 (1991).
[3] J. Y. Liu, X. X. Yu, G. H. Zhang, Y. K. Wu, K. Zhang, N. Pan, and X. P. Wang, Chin. J. Chem. Phys. **26**, 225 (2013).
[4] Y. S. Kim and W. P. Tai, Appl. Surf. Sci. **253**, 4911 (2007).
[5] J. C. Wang, F. C. Cheng, Y. T. Liang, H. I. Chen, C. Y. Tsai, C. H. Fang, and T. E. Nee, Nanoscale Res. Lett. **7**, 270 (2012).
[6] N. A. Estrich, D. H. Hook, A. N. Smith, J. T. Leonard, B. Laughlin, and J. P. Maria, J. Appl. Phys. **113**, 233703 (2013).
[7] J. Wen, C. Y. Zuo, M. Xu, C. Zhong, and K. Qi, Eur. Phys. J. B **80**, 25 (2011).
[8] S. Faÿ, J Steinhauser, N. Oliveira, E. V. Sauvain, and C. Ballif, Thin Solid Films **515**, 8558 (2007).
[9] X. G. Xu and H. L. Yang, Appl. Phys. Lett. **97**, 232502 (2010).
[10] G. Kim, J. Bang, Y. Kim, and S. K. Rout, Appl. Phys. A **97**, 821 (2009).
[11] X. L. Chen, B. H. Xu, J. M. Xue, Y. Zhao, C. C. Wei, J. Sun, Y. Wang, X. D. Zhang, and X. H. Geng, Thin Solid Films **515**, 3753 (2007).
[12] S. Y. Myong, J. Steinhauser, R. Schluchter, S. Fay, E. V. Sauvain, A. Shah, C. Ballif, and A. Rufenacht, Sol. Energy Mater. Sol. Cells **91**, 1269 (2007).
[13] J. Hu and R. G. Gordon, J. Electrochem. Soc. **139**, 2014 (1992).
[14] W. W. Wenas, A. Yamada, and K. Takahashi, J. Appl. Phys. **70**, 7119 (1991).
[15] W. W. Wenas, A. Yamada, M. Konagai, and K. Takahashi, Jpn. J. Appl. Phys. **30**, L441 (1991).
[16] B. N. Pawar, S. R. Jadkar, and M. G. Takwale, J. Phys. Chem. Solids **66**, 1779 (2005).
[17] B. J. Lokhande, P. S. Patil, and M. D. Uplane, Physica B **302**, 59 (2001).
[18] V. Kumar, R. G. Singh, F. Singh, and L. P. Purohit, J. Alloy Compd. **544**, 120 (2012).
[19] M. Caglara, S. Ilican, Y. Caglar, and F. Yakuphanoglu, J. Alloy. Compd. **509**, 3177 (2011).
[20] R. B. H. Tahar and N. B. H. Tahar, J. Mater. Sci. **40**, 5285 (2005).
[21] S. Jana, A. S. Vuk, A. Mallick, B. Orel, and P. K. Biswas, Mater. Res. Bull. **46**, 2392 (2011).
[22] V. Kumar, R. G. Singh, L. P. Purohit, and R. M. Mehra, J. Mater. Sci. Technol. **27**, 481 (2011).
[23] B. Wen, C. Q. Liu, W. D. Fei, H. L. Wang, S. M. Liu, N. Wang, and W. P. Chai, Chem. Res. Chin. Univ. **30**, 509 (2014).
[24] H. H. Huang, B. Orler, and G. L. Wilkes, Polym. Bull. **14**, 557 (1985).
[25] N. Wang, C. Q. Liu, B. Wen, H. L. Wang, S. M. Liu, and W. P. Chai, Mater. Lett. **122**, 269 (2014).
[26] A. E. Jiménez-González, J. A. Soto Urueta, and R. Suárez-Parra, J. Cryst. Growth **192**, 430 (1998).
[27] S. Ilican, Y. Caglar, and M. Caglar, J. Optoelectron. Adv. Mater. **10**, 2578 (2008).
[28] Y. Liao, X. Zhou, X. Xie, and Q. Yu, J. Mater. Sci. Mater. Electron. **24**, 4427 (2013).
[29] B. A. Kang, K. S. Hwang, and J. H. Jeong, J. Sol-Gel Sci. Technol. **43**, 145 (2007).

DOI:10.1063/1674-0068/29/cjcp1506116